Petroleum Science 21 (2024) 1002–1017

Contents lists available at ScienceDirect

Petroleum Science

journal homepage: www.keaipublishing.com/en/journals/petroleum-science

Original Paper

Fractal model of spontaneous imbibition in low-permeability reservoirs coupled with heterogeneity of pore seepage channels and threshold pressure

Ming-Sheng Zuo [a, b], Hao Chen [a, b, *], Xi-Liang Liu [a, b, **], Hai-Peng Liu [b], Yi Wu [b], Xin-Yu Qi [b]

[a] National Key Laboratory of Petroleum Resources and Engineering, China University of Petroleum (Beijing), Beijing, 102249, China
[b] College of Safety and Ocean Engineering, China University of Petroleum (Beijing), Beijing, 102249, China

ARTICLE INFO

Article history:
Received 8 June 2023
Received in revised form
27 October 2023
Accepted 30 October 2023
Available online 14 November 2023

Edited by Yan-Hua Sun

Keywords:
Spontaneous imbibition
Low-permeability reservoir
Fractal model
Threshold pressure
Capillary tube

ABSTRACT

Spontaneous imbibition (SI) is an important mechanism for enhancing oil recovery in low-permeability reservoirs. Due to the strong heterogeneity, and the non-Darcy flow, the construction of SI model for low-permeability reservoirs is extremely challenging. Commonly, traditional SI models based on single or averaged capillary tortuosity ignore the influence of heterogeneity of pore seepage channels and the threshold pressure (TP) on imbibition. Therefore, in this work, based on capillary model and fractal theory, a mathematical model of characterizing SI considering heterogeneity of pore seepage channels is established. On this basis, the threshold pressure was introduced to determine the pore radius at which the wetted phase can displace oil. The proposed new SI model was verified by imbibition experimental data. The study shows that for weakly heterogeneous cores with permeability of 0–1 mD, the traditional SI model can characterize the imbibition process relatively accurately, and the new imbibition model can increase the coefficient of determination by 1.05 times. However, traditional model has serious deviations in predicting the imbibition recovery for cores with permeability of 10–50 mD. The new SI model coupling with heterogeneity of pore seepage channels and threshold pressure effectively solves this problem, and the determination coefficient is increased from 0.344 to 0.922, which is increased by 2.68 times. For low-permeability reservoirs, the production of the oil in transitional pores (0.01–0.1 μm) and mesopores (0.1–1 μm) significantly affects the imbibition recovery, as the research shows that when the heterogeneity of pore seepage channels is ignored, the oil recovery in transitional pores and mesopores decreases by 7.54% and 4.26%, respectively. Sensitivity analysis shows that increasing interfacial tension, decreasing contact angle, oil–water viscosity ratio and threshold pressure will increase imbibition recovery. In addition, there are critical values for the influence of these factors on the imbibition recovery, which provides theoretical support for surfactant optimization.

1. Introduction

With the development of the petroleum industry, the recoverable reserves of conventional reservoirs have been declining year by year. Therefore, the exploration and development of low-permeability reservoirs have gradually become the focus of petroleum engineering. Low-permeability reservoirs typically have poor porosity, low permeability, small laryngeal radius, and significant heterogeneity (natural fractures development) (Higgs et al., 2007; Zou et al., 2012; Sun et al., 2019). Due to their strong heterogeneity, low-permeability reservoirs exhibit significant differences in permeability between microcracks and matrix. During the water flooding development of low-permeability reservoirs, water tends to move along high-permeability channels with lower flow resistance, resulting in a low waterflooding recovery rate (Allan and

* Corresponding author. National Key Laboratory of Petroleum Resources and Engineering, China University of Petroleum (Beijing), Beijing, 102249, China.
** Corresponding author. National Key Laboratory of Petroleum Resources and Engineering, China University of Petroleum (Beijing), Beijing, 102249, China.
E-mail addresses: Chenhaomailbox@163.com (H. Chen), xi_liang_liu@163.com (X.-L. Liu).

https://doi.org/10.1016/j.petsci.2023.10.027

Sun, 2003; Seethepalli et al., 2004). In recent years, many research results have shown that compared to water flooding, exploiting low-permeability reservoirs by spontaneous imbibition can significantly improve the recovery of low-permeability reservoirs, providing a new direction for achieving efficient development of low-permeability reservoirs (Xu et al., 2019; Das et al., 2019; Yassin et al., 2018).

Spontaneous imbibition refers to the displacement of a non-wetting phase (NWP) by a wetting phase (WP) through capillary forces in a porous medium (Morrow and Mason, 2001; Mirzaei-Paiaman et al., 2013). The process of spontaneous liquid infiltration into a substrate is primarily controlled by strong physical or chemical mechanisms such as capillary action, semi-wicking, or other related phenomena (Mason and Morrow, 2013). Lucas (1918) and Washburn (1921) regard the porous medium as a single capillary and establishes the Lucas–Washburn (L–W) equation to describe the process of spontaneous imbibition. Researchers have used imbibition experiments to demonstrate that imbibition recovery is influenced by multiple factors, including pore structure (Cao et al., 2022; Liu et al., 2020; Dai et al., 2019), reservoir wettability (Kalaei et al., 2013; Javaheri et al., 2018; Liu and Sheng, 2019), interfacial tension (IFT) (Adibhatla and Mohanty, 2008; Gupta and Mohanty, 2010), viscosity (Meng et al., 2017), and boundary conditions (Meng et al., 2019; Yang et al., 2021). The L–W model cannot provide a detailed explanation of the mechanism and controlling factors of imbibition recovery, thus underscoring its limitations and deficiencies in characterizing the imbibition recovery process.

Based on different mathematical methods, researchers have established numerous models to describe the SI process (Mason and Morrow, 2013), including the capillary tube model (Dong et al., 1998; Ruth and Bartley, 2011), continuum model (Adibhatla et al., 2005; El-Amin et al., 2013), and the pore network model (PNM) (Øren et al., 1998; Zhou et al., 2014) as the main ones. However, most of these models simplify the heterogeneity of pore geometry and pore structure, ignoring the influence of macro-heterogeneity and micro-pore throat structure on imbibition in low-permeability and tight reservoirs. Therefore, in recent years, based on molecular dynamics (Tian et al., 2021; Sang et al., 2022), lattice Boltzmann (LBM) (Porter et al., 2009; Leclaire et al., 2017), and dynamic network models (Al-Gharbi and Blunt, 2005; Tørå et al., 2012), researchers have further studied the influence of micro-nano pores and heterogeneity on imbibition rules. But the MD method is only suitable for simulating SI processes with short time intervals in the nano-scale. LBM can simulate SI in complex nano-scale pore structures, but its computational demands make it impractical for rock core. The dynamic network models face modeling and computational difficulties in characterizing spontaneous imbibition (Lux and Anguy, 2012).

Low-permeability reservoirs is composed of numerous micro-nano pores, and the pore structure is highly complex and heterogeneous, making it difficult to represent the pore structure parameters in Euclidean geometry. It has been demonstrated that the pore spaces of many natural porous media exhibit fractal characteristics, meaning that they are self-similar at multiple scales (Yu et al., 2002). With the application of techniques such as nuclear magnetic resonance (NMR), mercury injection capillary pressure (MICP) testing, X-ray computed tomography (X-CT) and other technologies, fractal theory has been extensively studied (Katz and Thompson, 1985; Cai and Yu, 2010) and widely used to describe the complex pore structure parameters (Li, 2010; Yu and Cheng, 2002) and fluid flow characteristics of reservoirs (Buiting and Clerke, 2013; Wang et al., 2017).

Yu (2008) summarized the fractal theory application parameters (pore microstructures, tortuosity of flow paths, fractal dimensions, flow resistances) of fluid flow and transport properties in porous media. Cai and Yu (2011) has derived the tortuosity of capillaries based on fractal theory and coupled it with the L–W equation to obtain a fractal SI model. They discussed the influence of capillary tortuosity on the spontaneous imbibition in porous media, and the research showed that the time exponent of spontaneous imbibition varies between 0.5 and 0.167. Based on this, Cai et al. (2012) derived a complete analytical expression for the spontaneous imbibition of wetting fluid in porous media considering gravity. The model considers contact area, porosity, pore fractal dimension, pore throat radius, fluid properties (density, viscosity), and provides a reasonable explanation for the influence of gravity on imbibition and recovery efficiency.

Based on the fractal theory, Wang and Zhao (2019) proposed a characterizing co-current SI of water into oil-saturated tight sandstone. This model dynamically characterizes the imbibition rate of pores with different sizes and the inhomogeneity of imbibition front, and analyzes the influence of wettability and interfacial tension on imbibition recovery. Salam and Wang (2022) used fractal theory to establish an imbibition model considering the capillary surface roughness of a single tortuosity and fluid viscosity. The research shows that the increases in surface roughness and fluid effective viscosity lead to the decrease in imbibition recovery. Zhu et al. (2022) investigated the influence of non-Newtonian fluids on the imbibition rule through fractal theory. Their study shows that when the wetting phase is a non-Newtonian fluid, there is a nonlinear relationship between the imbibition distance and the square root of time. Li et al. (2022) found that the use of fractal theory can greatly simplify the calculation process of tight sandstone imbibition when studying the influence of mixed-wet pore surface on imbibition recovery. The existing SI models based on fractal theory usually use the single or average pore tortuosity, ignoring the heterogeneity of capillary tortuosity with different pore radius, resulting in some discrepancies when fitting with experimental data of the low-permeability imbibition.

In 1963, Miller and Low (1963) proposed for the first time that the interaction between adsorbed molecules and solid molecules led to the existence of a driving condition through a large number of percolation experiments in low-permeability porous media, and called this driving condition the threshold pressure gradient (TPG). Prada and Civan (1999) found that the threshold pressure gradient of a single-phase fluid is a parameter related to permeability and fluid viscosity through core displacement experiments, and proposed a non-Darcy flow model that considers the threshold pressure gradient. Based on the fractal theory, Chen et al. (2022) proposed a non-Darcy seepage model considering the thickness of the boundary layer, and analyzed the correlation between the permeability and the threshold pressure gradient in low-permeability reservoirs. Gao et al. (2021) elucidated the effect of micro-nano pore threshold pressure on seepage in tight oil reservoirs from a molecular perspective. Numerous laboratory and field experiments (Bauer et al., 2019; Tian et al., 2018; Li et al., 2016) have shown that there is a threshold pressure gradient in low-permeability reservoirs, which impedes the fluid flow. The threshold pressure should not be ignored when studying the flow of low-permeability and tight reservoirs. But the effect of threshold pressure gradient on imbibition enhanced recovery in low-permeability reservoirs, there are few studies available in the current literature and imbibition models regarding this aspect.

Based on the basic fractal characteristics of porous media microstructure, this paper considers the heterogeneity of pore seepage channels and threshold pressure to derive the imbibition fractal model. Compared to previous fractal SI models that considered only single/average capillary tortuosity, the new SI model provides a more accurate characterization of imbibition in

low-permeability reservoir. Based on the new imbibition model, the effects of wettability, IFT, oil viscosity and threshold pressure on imbibition recovery of low-permeability reservoir were analyzed. The purpose of the article is to provide proper guidance for the mechanism of imbibition enhanced oil recovery in low-permeability reservoirs.

2. Experimental

2.1. The threshold pressure gradient measurement

In this paper, the threshold pressure gradients of 5 rock cores with different permeability values were tested using the pressure balance method. An empirical formula was fitted to describe the relationship between threshold pressure and permeability by experimental results of the threshold pressure gradient. In this paper, the threshold pressure of the new SI model will be calculated based on this empirical formula.

2.1.1. Rock and fluid properties

The parameters of the core samples used are shown in Table 1. The oil used was a mixture of crude oil from an offshore block in China and kerosene in a volume ratio of 1:3. The oil had a density of 0.84 g/cm^3 and a viscosity of 3.62 mPa s at 25 °C.

2.1.2. Experimental equipment and procedure

In the experiment, a SYS-III multi-stage high temperature and high pressure displacement system was used to measure the threshold pressure gradient, and the experimental flow chart is shown in Fig. 1. The experimental equipment mainly includes an ISCO high-precision displacement pump with a pressure accuracy of 0.05 MPa and a flow velocity accuracy of 0.001 mL/min, a high-pressure core holder, and a high-precision pressure monitoring system with an accuracy of 0.0001 MPa.

Experimental procedure is as follows:

(1) The core is vacuumed for 24 h to remove residual air. Then, an experimental simulation oil is injected into the saturation cell, and the rock core is saturated for 48 h under a saturation pressure of 20 MPa.
(2) Put the core into the core holder and apply a confining pressure of 2 MPa to the core. Use the ISCO pump to apply a pressure of 1 MPa to the intermediate container, and obtain the flow rate of the fluid inside the core through the flow meter at the end of the core holder.
(3) When the flow of oil in the core reaches a steady state, keep the upstream pressure constant, and turn off the switch at the outlet of the core holder.
(4) Record the downstream pressure every 2 h. Stop the experiment when the downstream pressure is stable and no longer changes (three consecutive errors are less than 4%). The difference between the upstream constant pressure and the stable downstream pressure is the threshold pressure.
(5) Repeat steps (1)–(4) to measure the threshold pressure gradient of cores with different permeability.

Table 1
Petrophysical properties of core samples.

Core No.	Diameter, cm	Length, cm	Porosity, %	Permeability, mD
1	2.52	5.02	10.03	0.26
2	2.53	4.95	10.62	1.14
3	2.53	4.86	11.66	5.25
4	2.51	4.97	13.03	10.12
5	2.49	5.13	18.03	20.62

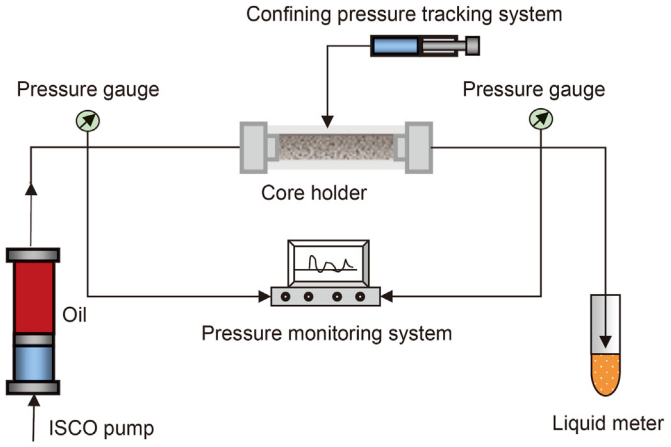

Fig. 1. Schematic diagram for measuring threshold pressure gradient.

2.1.3. Experimental results

According to the experimental data, the relationship between threshold pressure gradient and permeability is drawn, as shown in Fig. 2. As the core permeability increases, the threshold pressure gradient decreases. The empirical formula for the threshold pressure gradient and permeability is established using power function fitting, as shown in Eq. (1).

$$P_{TPG} = 0.7406K^{-1.222} \quad (1)$$

where K is the permeability of the core, mD; P_{TPG} is the threshold pressure gradient, MPa/m.

2.2. Spontaneous imbibition experiments

The core 4 in the threshold pressure gradient experiment was selected to carry out the imbibition experiment. The oil used in the imbibition experiment was the same as that used in the threshold pressure experiment and use a 0.1% AEO surfactant as the imbibition solution.

2.2.1. Rock and fluid properties

The parameters of the core sample are shown in Table 1. The IFT between 0.1% AEO solution and oil was measured at 25 °C and atmospheric pressure (0.1 MPa) using a rotating interfacial tension instrument TX-500C. The wettability of the rock surface was characterized by contact angle. The contact angle of the core 4 was measured using the data physics equipment from Geno USA.

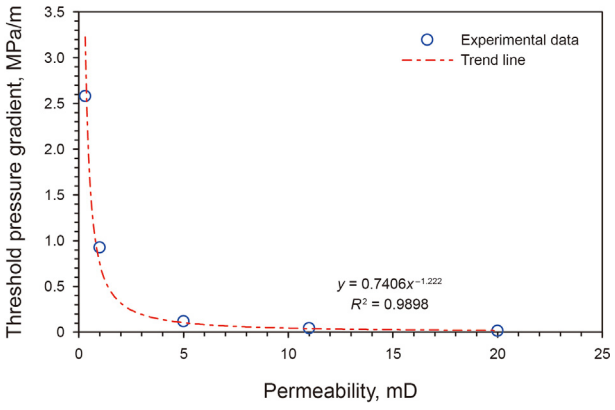

Fig. 2. Relationship between threshold pressure gradient and permeability.

The IFT between AEO solution and oil is 2.23 mN/m and the contact angle of the core is 88°.

2.2.2. Experimental steps

The core saturated with oil was placed in the Amott cell containing a surfactant solution of 0.1% AEO, as shown in Fig. 3. Under the action of buoyancy, the oil droplets recovered during the imbibition process will float to the top of the Amott cell, and the amount of the oil recovered by spontaneous imbibition is obtained by reading the scale on the top of the Amott cell. The imbibition recovery of the core was recorded every 6 h.

3. Methodology

3.1. Fractal theory for porous media

The microstructure of pore size distribution can be characterized with fractal theory (Yu and Cheng, 2002). The number of pores with radius greater than r and less than r_{max} satisfies power-law relation:

$$N(n \geq r) = \left(\frac{r_{max}}{r}\right)^{D_f} \tag{2}$$

where $N(n \geq r)$ is the number of pores, dimensionless; r is the pore radius, μm; n is any pore radius that is larger than r, μm; r_{max} is the maximum pore radius, μm; D_f is the fractal dimension, and the range of D_f in the two-dimensional space is $0 < D_f < 2$.

Differentiate Eq. (2) to derive the pore number with the pore radius varying between r and $r + dr$:

$$-dN = D_f r_{max}^{D_f} r^{-(D_f+1)} dr \tag{3}$$

For the core with the diameter d (μm) and porosity ϕ, the number of pores with the pore radius varying between r and $r + dr$ on the cross-section of the core can be expressed as

$$-dN = \frac{(2 - D_f)\phi d^2}{4(1-\phi) r_{max}^{2-D_f}} r^{-(D_f+1)} dr \tag{4}$$

where $-dN > 0$ indicates that the number of pores decreases with the increase in radius. D_f can be calculated by Eq. (5):

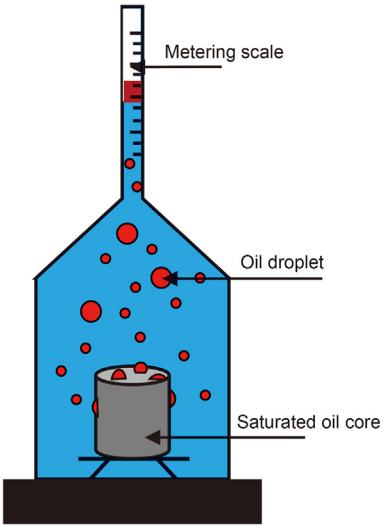

Fig. 3. Schematic diagram of SI experiment with an Amott cell.

$$D_f = d_E - \frac{\ln\phi}{\ln(r_{min}/r_{max})} \tag{5}$$

where d_E is the space size of the Euclidean geometry. In the two-dimensional space, $d_E = 2$; $1 < D_f < 2$; r_{min} is the minimum pore radius, μm; ϕ is the porosity.

Interconnecting pore-throats are like curved capillaries and are usually quantified by the tortuosity in the reservoir. Cai and Yu (2011) argued that the diameter of capillaries is analogous to the length scale (λ), and they developed the fractal scaling relationship between the actual distance and the diameter of capillaries in porous media, as shown in Eq. (6):

$$L_f(\lambda) = L_s^{D_T} \lambda^{1-D_T} \tag{6}$$

where L_f is the actual channel of the tortuous capillary, μm; L_s is the characteristic length of the tortuous capillary, which is also the straight-line imbibition distance, μm; λ is the pore diameter, μm; D_T is the fractal dimension of tortuosity.

The fractal dimension D_T of a curved capillary in porous media can be expressed as

$$D_T = 1 + \frac{\ln\tau_{av}}{\ln(L_s/\lambda_{av})} \tag{7}$$

where τ_{av} is the average tortuosity of the curved capillary; λ_{av} is the average pore diameter, μm.

Yu and Li (2004) derived a simple geometry model for tortuosity of flow paths in porous media based on the two configurations, as shown in Eq. (8):

$$\tau_{av} = \frac{1}{2}\left[1 + \frac{1}{2}\sqrt{1-\phi} + \sqrt{1-\phi}\,\frac{\sqrt{\left(\frac{1}{\sqrt{1-\phi}} - 1\right)^2 + \frac{1}{4}}}{1 - \sqrt{1-\phi}}\right] \tag{8}$$

Xu and Yu (2008) deduced the geometric models of L_s, as shown in Eq. (9):

$$L_s = \frac{\lambda_{max}}{\lambda_{min}} \frac{D_f - 1}{\sqrt{D_f}} \sqrt{\frac{\pi}{2 - D_f} \frac{1-\phi}{4\phi}} \lambda_{av} \tag{9}$$

where λ_{max} is the maximum pore diameter, μm; λ_{min} is the minimum pore diameter, μm;

By substituting Eqs. (7) and (9) into Eq. (6) the actual channel of the tortuous capillary can be calculated.

3.2. SI model considering heterogeneity of pore seepage channels

The research object is oil and water in the capillary tube. According to the Newton second theory, the location of the interface between water and oil during the co-current SI process in a capillary tube can be calculated as follows (Wu et al., 2021):

$$x(r,t) = \frac{-\mu_o L_f + \sqrt{\left(\mu_o L_f\right)^2 + (\mu_w - \mu_o)(\sigma r t \cos\theta)\Big/2}}{\mu_w - \mu_o} \tag{10}$$

where $x(r, t)$ is the imbibition interface location; r is the capillary tube radius, μm; μ_o is the oil viscosity, mPa s; μ_w is the water viscosity, mPa s; σ is the IFT between oil and water, mN/m; t is the imbibition time, s; θ is the contact angle, degree.

By substituting Eq. (6) into Eq. (10), the oil–water interface in capillaries with different pore throat radius at different times during the imbibition process can be obtained

$$x(r,t)=\frac{-\mu_o L_s^{D_T}(2r)^{1-D_T}+\sqrt{\left(\mu_o L_s^{D_T}(2r)^{1-D_T}\right)^2+(\mu_w-\mu_o)(\sigma r t\cos\theta)\Big/2}}{\mu_w-\mu_o} \tag{11}$$

The oil production by the imbibition at time t can be calculated by

$$Q(t)=-\int_{r_{min}}^{r_{max}}\pi r^2 x(r,t)\mathrm{d}N=\frac{\pi\left(2-D_f\right)\phi d^2}{4(1-\phi)r_{max}^{2-D_f}}\int_{r_{min}}^{r_{max}} r^{1-D_f}x(r,t)\mathrm{d}r \tag{12}$$

The connate water is distributed in the pores of the low-permeability reservoir. According to assumptions of Wang and Zhao (2019) the thickness ratio of the immovable boundary-layer to the capillary tube radius is the same for every capillary tube. The effective radius for the imbibition flow is reduced to

$$r_e=r-h_w=r\sqrt{1-S_w} \tag{13}$$

where r_e is the effective flow radius, μm; h_w is the thickness of connate water, μm; S_w is the irreducible water saturation.

Submitting Eq. (13) into Eq. (12), the oil production by the imbibition with immovable connate water can be expressed as

$$Q(t)=\frac{\pi\left(2-D_f\right)\phi d^2}{4(1-\phi)r_{max}^{2-D_f}}(1-S_w)^{\frac{D_f}{2}}\int_{r_{min}\sqrt{1-S_w}}^{r_{max}\sqrt{1-S_w}}(r_e)^{1-D_f}x(r_e,t)\mathrm{d}r_e \tag{14}$$

Due to the consideration of heterogeneity of pore seepage channels, the seepage length and flow resistance of the capillary in different pores are different. Therefore, the end time of imbibition of the capillary with different pores is different. During the process of imbibition, at time t, the imbibition can be divided into two situations at different pore radii of capillary: (1) imbibition has been completed and (2) still in the imbibition stage.

When calculating the total oil production, Eq. (11) for imbibition time t will be changed to a piecewise function:

$$x(r_e,t)=\begin{cases}\dfrac{-\mu_o(2r_e)^{1-D_T}(1-S_w)^{\frac{D_T-1}{2}}L_s^{D_T}+\sqrt{{\mu_o}^2(2r_e)^{2-2D_T}(1-S_w)^{D_T-1}L_s^{2D_T}+(\mu_w-\mu_o)\dfrac{\sigma\cdot r_e\cdot\cos\theta\cdot t}{2}}}{\mu_w-\mu_o} & t<t_E(r_e)\\ 2^{1-D_T}{L_s}^{D_T}r_e^{2-D_f-D_T} & t\geq t_E(r_e)\end{cases} \tag{15}$$

where $t_E(r)$ is the imbibition ending time of different radii, s.

Submitting Eq. (15) into Eq. (14), we can get the oil production by the imbibition. When the $t<t_E(r_e)$, Eq. (16) is used to calculate the oil production $Q_1(t)$.

$$Q_1(t)=\frac{\pi\left(2-D_f\right)\phi d^2}{4(1-\phi)r_{max}^{2-D_f}}(1-S_w)^{\frac{D_f}{2}}\times\int_{r_{min}\sqrt{1-S_w}}^{r_t\sqrt{1-S_w}}{r_e}^{1-D_f}\left(\frac{-\mu_o(2r_e)^{1-D_T}(1-S_w)^{\frac{D_T-1}{2}}L_s^{D_T}}{\mu_w-\mu_o}+\frac{\sqrt{{\mu_o}^2(2r_e)^{2-2D_T}(1-S_w)^{D_T-1}L_s^{2D_T}+(\mu_w-\mu_o)\frac{\sigma\cdot r_e\cdot\cos\theta\cdot t}{2}}}{\mu_w-\mu_o}\right)\mathrm{d}r_e \tag{16}$$

When $t\geq t_E(r_e)$, Eq. (17) is used to calculate the oil production $Q_2(t)$.

$$Q_2(t)=\frac{\pi\left(2-D_f\right)\phi d^2}{4(1-\phi)r_{max}^{2-D_f}}(1-S_w)^{\frac{D_f+D_T-1}{2}}\int_{r_t\sqrt{1-S_w}}^{r_{max}\sqrt{1-S_w}}2^{1-D_T}L_s^{D_T}r_e^{2-D_f-D_T}dr_e \tag{17}$$

At any time t, the total oil production by imbibition is $Q_1(t)+Q_2(t)$, as shown in Eq. (18):

$$Q(t)=Q_1(t)+Q_2(t) \tag{18}$$

where r_t represents the pore radius that has completed imbibition at time t, μm.

The imbibition end times of seepage channels with different pore radii are different. In recovery calculations using Eqs. (16) and (17), the pore radius r_t changes with time. Therefore, when calculating the imbibition recovery at a specific time, it is necessary to first determine the pore radius that has completed imbibition at that time. When the location of imbibition interface reaches the end of the capillary tube, the SI is over. The imbibition ending time $t_E(r)$ can be determined by submitting $x(r, t)=L_f$ into Eq. (10):

$$t_E(r)=\frac{2(\mu_o+\mu_w)L_f^2}{\sigma r\cos\theta} \tag{19}$$

Submitting Eqs. (6) and (13) into Eq. (19), the ending imbibition time of capillary with different pore radius, considering the connate water can be obtained

$$t_E(r_e)=\frac{2^{3-2D_T}(\mu_o+\mu_w)(1-S_w)^{D_T-1}L_s^{2D_T}r_e^{1-2D_T}}{\sigma r_e\cos\theta} \tag{20}$$

According to Eqs. (13) and (20), the capillary pore radius (r_t) that completes imbibition at time t can be deduced

$$r_t=\left(\frac{2^{3-2D_T}(\mu_o+\mu_w)(1-S_w)^{-D_T}L_s^{2D_T}}{\sigma\cos\theta\cdot t}\right)^{\frac{1}{2D_T-1}}\times\frac{1}{\sqrt{1-S_w}} \tag{21}$$

Submitting the calculation result of Eq. (21) into Eqs. (16) and (17), the imbibition oil production can be calculated.

The oil recovery factor at time t can be calculated by

$$R(t)=\frac{4Q(t)}{\pi d^2h\phi(1-S_w)}\times 100\% \tag{22}$$

where d is the core diameter, cm; h is the core length, cm; $R(t)$ is the oil recovery factor, %.

Based on fractal theory and capillary bundle model, a SI model considering heterogeneity of pore seepage channels was constructed.

3.3. SI model considering the threshold pressure

In low-permeability reservoirs, the threshold pressure of the fluid is the resistance. Therefore, when the pressure of the capillary bundles (P_{nc}) is higher than the threshold pressure (P_{TP}), the wetting phase can drive the oil in the pore.

Based on the number of pores with different pore radii calculated by fractal theory (Eq. (4)) and the capillary force of pore radius (Eq. (23)), the driving force of capillary bundles with different pore radii is obtained, as shown in Eq. (24):

$$P_c=\frac{2\sigma\cos\theta}{r} \tag{23}$$

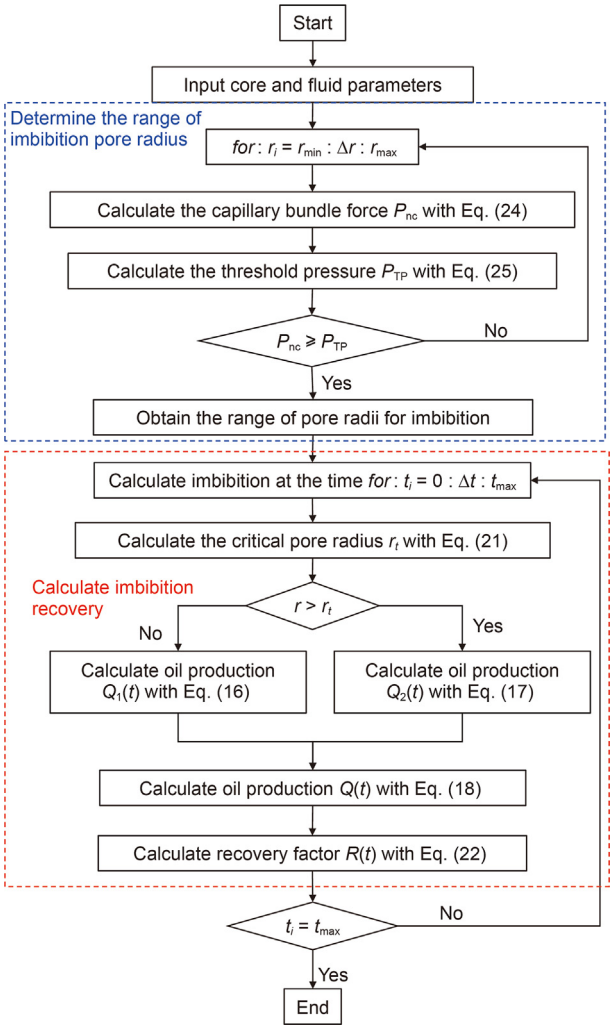

Fig. 4. Flowchart for the new SI model proposed in this paper.

$$P_{nc}=P_c dN=\frac{\left(2-D_f\right)\phi d^2}{2(1-\phi)r_{max}^{2-D_f}}r^{-(D_f+2)}\sigma\cos\theta dr \tag{24}$$

where P_c is the capillary force, kPa; P_{nc} is the pressure of the capillary bundles, kPa.

The threshold pressure is calculated based on the empirical equation (Eq. (1)):

$$P_{TP}=P_{TPG}h=0.7406K^{-1.222}h/100 \tag{25}$$

where P_{TP} is the threshold pressure, MPa.

When $P_{nc} > P_{TP}$, the oil within the pore radius r is displaced under the capillary driving force. When $P_{nc} < P_{TP}$, the capillary force cannot displace the oil in the pore radius r.

$$P_{nc}>P_{TP}:\left(\frac{\left(2-D_f\right)\phi d^2}{2(1-\phi)r_{max}^{2-D_f}}\times\frac{\sigma\cdot\cos\theta\cdot dr\cdot 100\cdot K^{1.222}}{0.7406\cdot h}\right)^{-D_f-2}>r \tag{26}$$

Using numerical methods to solve Eq. (26), we can obtain the upper limit of the pore radius of capillary bundle that overcomes the threshold pressure.

Table 2
Properties of core samples and fluids from the literature used for model validation.

Core No.	d, cm	L, cm	ϕ, %	k, mD	r_{max}, μm	r_{min}, μm	r_{avg}, μm	θ, degree	IFT, mN/m	μ_w, mPa s	μ_o, mPa s	Reference
L1	2.46	2.53	6.52	0.0054	0.0982	0.001	0.00864	86.0	18.96	1.00	2.21	Wu et al., 2017
L2	2.53	5.04	12.25	0.47	0.429	0.001	0.078	48.7	9.78	2.47	7.97	Cheng et al., 2018
L3	2.49	6.19	10.85	1.38	2.733	0.001	0.481	65.7	1.21	1.00	2.90	Wang et al., 2022
L4	2.51	5.00	12.31	1.25	2.249	0.001	0.342	45.0	0.15	1.00	1.34	You et al., 2018
L5	3.8	7.45	28.23	14.43	8.617	0.0015	1.165	78.0	6.71	1.00	3.90	Gupta and Mohanty, 2010
L6	3.83	7.18	13.64	56.81	12.858	0.0015	3.474	68.6	0.12	0.39	3.60	Souayeh et al., 2021

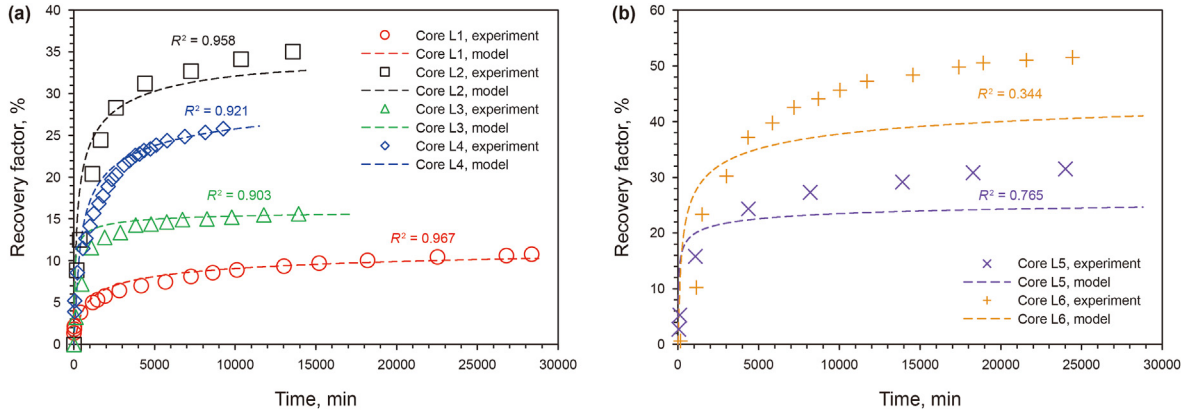

Fig. 5. Oil recovery factor versus time from the SI experiments in the literature and previous SI without considering the heterogeneity of pore channels. (**a**) Core permeability of 0.0054–1.38 mD; (**b**) Core permeability of 14.43 and 56.81 mD.

As shown in Fig. 4, a computer code was developed to calculate the imbibition recovery. Firstly, the pore radius range of imbibition is determined according to the threshold pressure. Then the calculation of imbibition recovery at different times based on imbibition formula derived from the fractal theory and the capillary tube model.

4. Results and discussion

4.1. Validation of the previous SI model constructed based on average tortuosity

There are many studies of SI (Wu et al., 2017; Cheng et al., 2018; Wang et al., 2022; You et al., 2018; Gupta and Mohanty, 2010; Souayeh et al., 2021) and the SI experimental method and steps used in the literature are nearly identical to the imbibition experiment in this paper. The parameters of core samples and fluids used in the literature are listed in Table 2.

Eq. (27) can be used to calculate the length L_f of the average tortuosity seepage capillary channel. Replacing Eq. (6) with Eq. (27) and submitting it to the SI model, we can obtain the SI model proposed by previous researchers that does not consider the heterogeneity of pore seepage channels.

$$L_f = \tau_{av} L_s \tag{27}$$

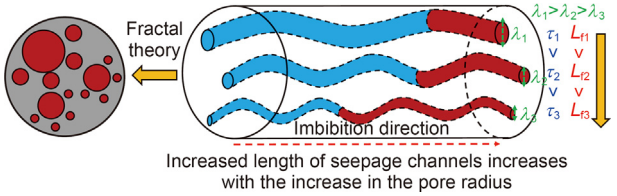

Fig. 6. Relationship between physical properties of pore seepage channels and pore scale.

According to the parameters of the cores and the imbibition fluids provided in the literature, the imbibition process of the cores in Table 2 was simulated using the previous SI model that didn't consider heterogeneity of pore seepage channels, and compared with the experimental data, as shown in Fig. 5.

When the core permeability ranges from 0.0054 to 1.38 mD, the previous SI model relatively accurately characterizes the SI process of core experiments, as shown in Fig. 5(a). The range of determination coefficient is 0.903–0.967. When the core permeability reaches 14.4 mD, the prediction of core imbibition process by the previous SI model appears obvious deviation, and the determination coefficient is 0.765, as shown in Fig. 5(b). When the core permeability reaches 56.81 mD, the previous SI model cannot correctly simulate the imbibition recovery, the determination coefficient is 0.344, as shown in Fig. 5(b).

The determination coefficient shows that for the previous SI model, the determination coefficient gradually decreases with the increase in the core permeability. Therefore, the previous SI model constructed by single/average capillary tortuosity is no longer applicable for the prediction of imbibition recovery in low permeability reservoirs (permeability 10–50 mD).

As shown in Eq. (6), the calculation formula of the capillary channels shows that the pore radius has a power function relationship with the capillary length. Therefore, the differences in the capillary seepage channels of different pore sizes, such as their length and tortuosity, can significantly affect the contribution to SI recovery, as shown in Fig. 6. In this paper, it is considered that ignoring heterogeneity of pore seepage channels is one of the reasons why previous SI model cannot accurately predict imbibition recovery in low-permeability reservoirs.

Base on the fractal theory and the capillary force formula, as shown in Eq. (24), increasing the pore radius will greatly reduce the capillary force and lead to a decrease in the pore number at the same time. Therefore, in some large pores, when the capillary force is less than the threshold pressure, the oil inside cannot be recovered. In this paper, it is believed that the influence of threshold

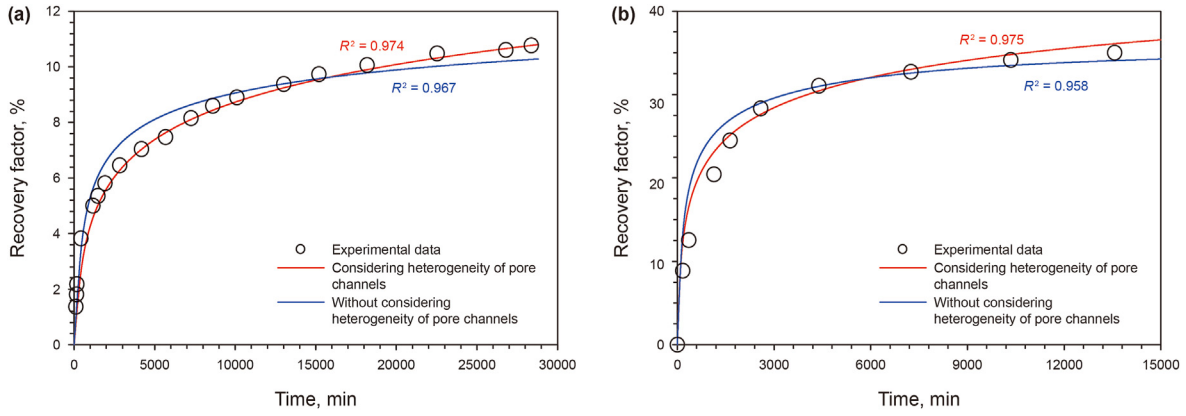

Fig. 7. Comparison of the imbibition profiles of SI recovery versus time between previous model and new model in the cores with permeability of 0.0054 mD (**a**) and 0.47 mD (**b**).

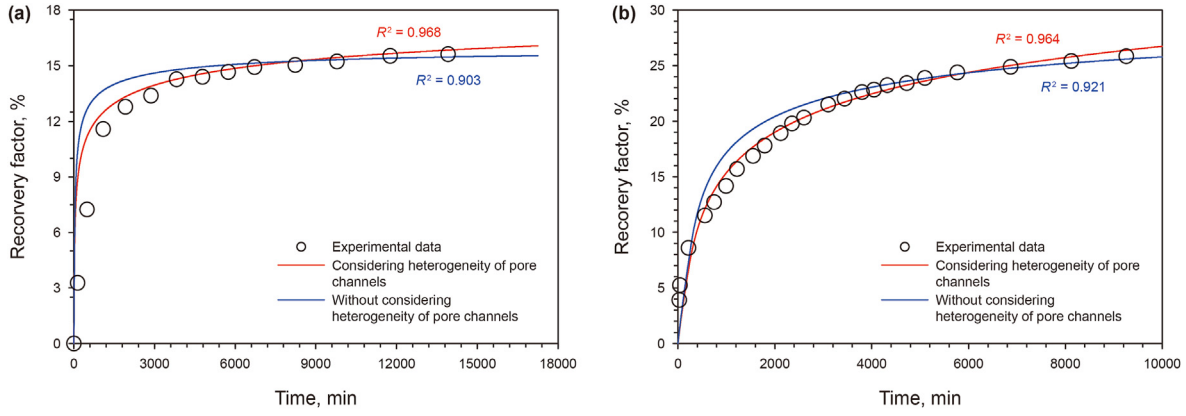

Fig. 8. Comparison of the imbibition profiles of SI recovery versus time between previous model and new model in the cores with permeability of 1.38 mD (**a**) and 1.25 mD (**b**).

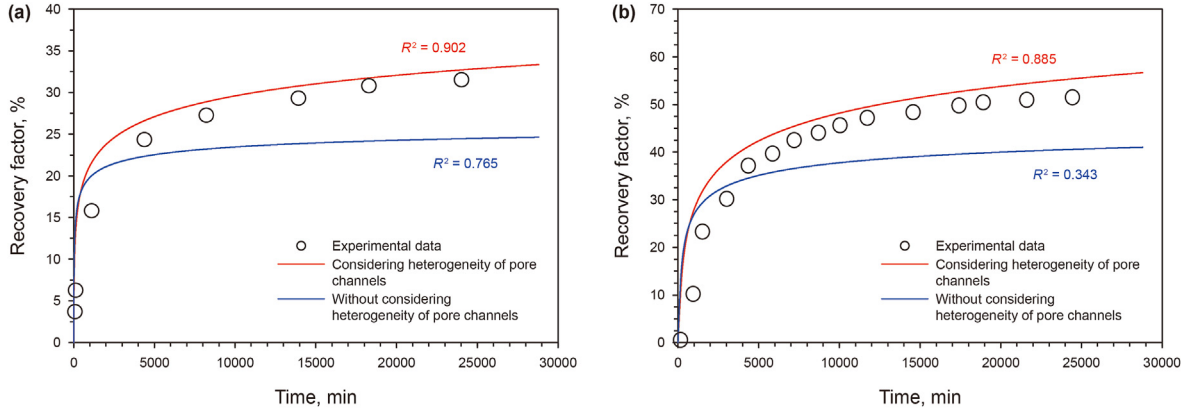

Fig. 9. Comparison of the imbibition profiles of SI recovery versus time between previous model and new model in the cores with permeability of 14.43 mD (**a**) and 56.81 mD (**b**).

pressure on oil production in pores is not considered, which is the second reason why the previous SI model cannot accurately predict imbibition recovery.

4.2. Influence of heterogeneity of pore seepage channels on SI model

According to the new SI model considering heterogeneity of pore seepage channels constructed in this paper, and based on the SI experimental data in the literature, the accuracy of the new SI model in simulating the SI process of cores with different physical properties was studied. In addition, the simulation results of SI models with and without considering the heterogeneity of pore seepage channels were compared and analyzed.

As shown in Fig. 7, the core permeability is 0.0054 and 0.47 mD, respectively. The determination coefficients of the previous SI model without considering the heterogeneity of pore seepage channels are 0.967 and 0.958, respectively. For the new SI model considering the heterogeneity of pore seepage channels, the determination coefficients of the new SI model are increased by

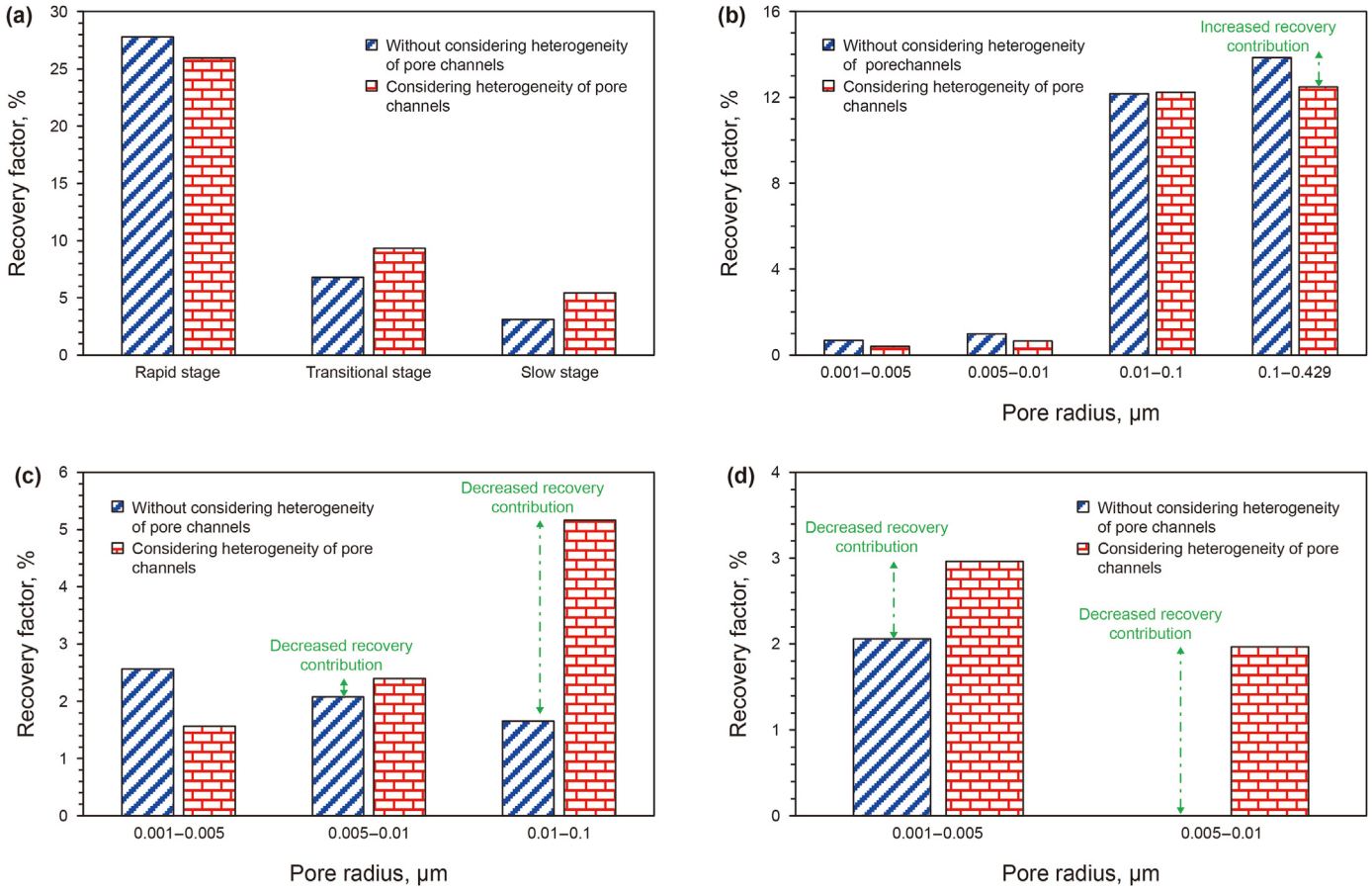

Fig. 10. Comparison of the calculation results of oil recovery in different pores at different SI stages between previous model and new model, in the core with permeability of 0.47 mD. (**a**) Oil recovery at different imbibition stages. Oil recovery in different pores in rapid stage (**b**), transitional stage (**c**), and slow stage (**d**).

1.01 and 1.02 times, respectively. Research has shown that although both models can fit the experimental data well, the new model that considers heterogeneity of pore seepage channels performed better, especially in the early stages of imbibition.

As shown in Fig. 8, the core permeability is 1.38 and 1.25 mD, respectively. The determination coefficients of the previous SI model without considering the heterogeneity of pore seepage channels are 0.903 and 0.921. After considering the heterogeneity of pore seepage channels, the determination coefficients increased to 0.968 and 0.964, respectively.

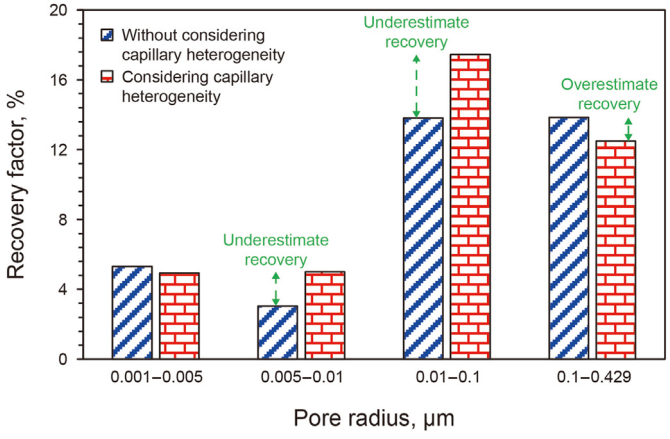

Fig. 11. Oil recovery in pores of different radii (0.001–0.429 μm) during SI.

The results indicate that when the core permeability increases from 0.0054 to 1.38 mD, the determination coefficient of previous imbibition model decreases up to 6.61%. However, the increase in core permeability had little effect on the prediction accuracy of the new SI model. In addition, the new model improved the coefficient determination of the previous model by 1.07 times.

As shown in Fig. 9, the core permeability is 14.43 and 56.81 mD, respectively. The determination coefficients of the previous SI model are poor, only 0.765 and 0.343. The determination coefficients of the new SI model considering the heterogeneity of pore seepage channels are 0.902 and 0.885, respectively.

The new SI model improves the determination coefficient of the previous imbibition model by 1.18 and 2.58 times, respectively. This shows that after considering the heterogeneity of pore seepage channels, it effectively addresses the problems encountered in the previous SI model.

In order to further clarify the influence of heterogeneity of pore seepage channels on imbibition recovery, based on SI models with and without considering heterogeneity of pore seepage channels, for core L2 and core L5, the contribution of different pores at different imbibition stages to recovery was studied.

According to previous research results, the process of imbibition enhanced oil recovery (I-EOR) can be divided into three stages: rapid stage, transitional stage, and slow stage. And according to the size of the pore radius, they divided the reservoir pore radius into four categories (Lu et al., 2018): micropores (0.001–0.01 μm), transitional pores (0.01–0.1 μm), mesopores (0.1–1 μm), and

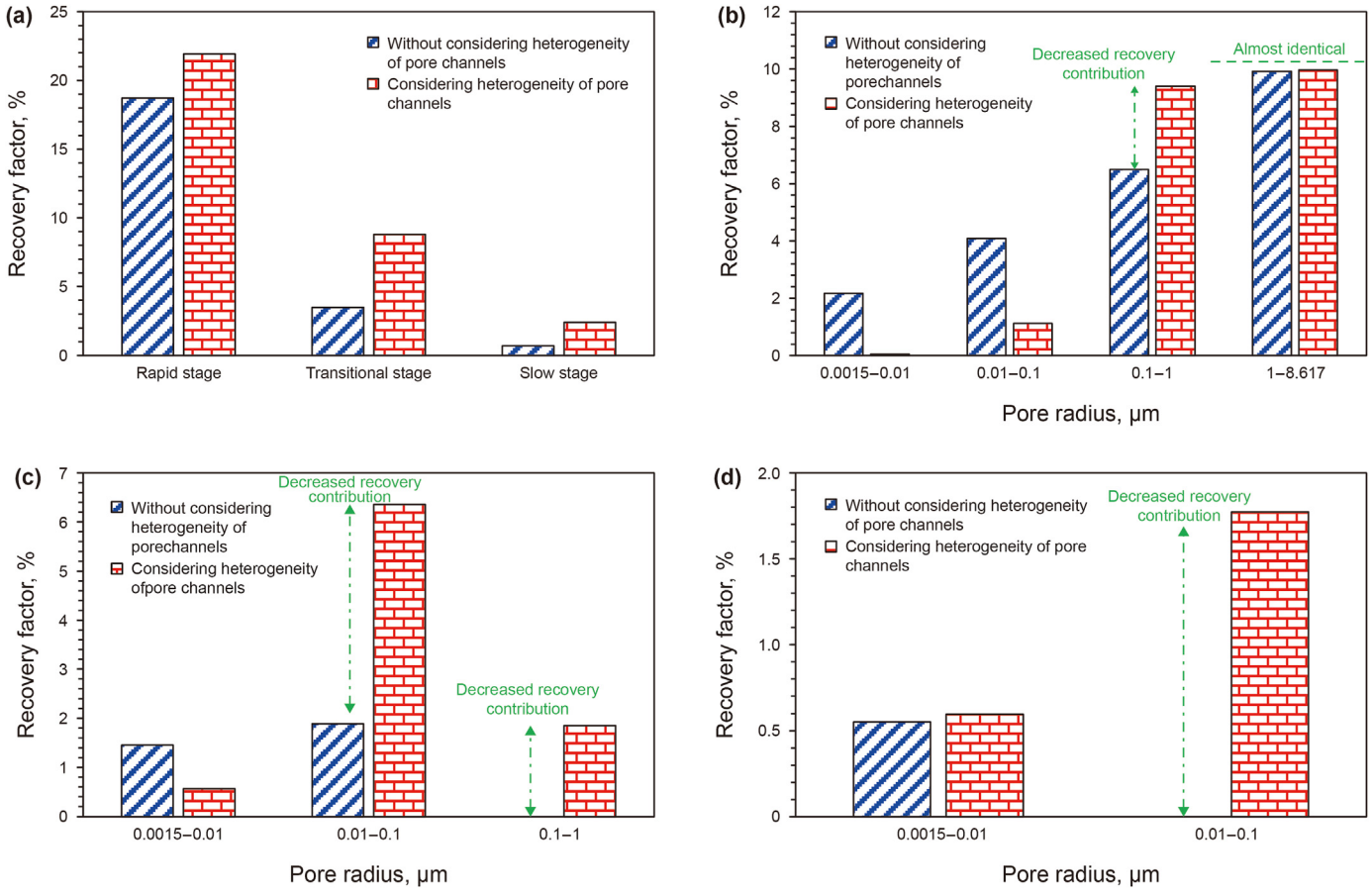

Fig. 12. Comparison of the imbibition profiles of new model and previous model for core permeability of 14.43 mD. (**a**) Oil recovery at different imbibition stages. Oil recovery in different pores in rapid stage (**b**), transitional stage (**c**), and slow stage (**d**).

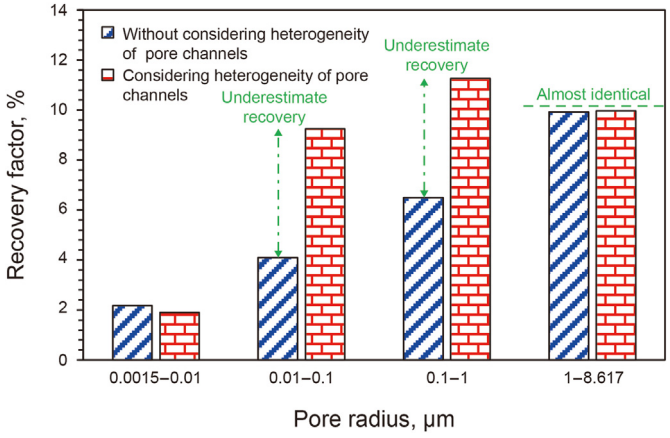

Fig. 13. Oil recovery in pores of different radii (0.0015–8.617 μm) during SI.

macropores (>1 μm).

The previous and new models were used to calculate the oil production of core L2 in different SI stages and different pores, as shown in Fig. 10. In the rapid imbibition stage, as shown in Fig. 10(a), the previous imbibition model (without considering heterogeneity of pore seepage channels) overestimated the capillary volume of the mesopores (0.1–0.429 μm), resulting in a 1.38% increase in the contribution of the mesopores to imbibition recovery. In the transitional and slow stages of imbibition, as shown in Fig. 10(c) and (d), if the heterogeneity of pore seepage channels is neglected, the calculated contributions of transitional pores (0.01–0.1 μm) and micropores (0.001–0.01 μm) to imbibition recovery are reduced by 3.58% and 2.21%, respectively.

For cores with permeability of 0.0054–1.38 mD, studies have proved that if the heterogeneity of pore seepage channels is ignored, this will overestimate oil recovery in mesopores and underestimate oil recovery in transitional pores and micropores, which is the reason for the low determination coefficient of previous SI model, as shown in Fig. 11.

The calculation results of the previous and new models for the recovery of oil in different pores at different stages of core L5 (permeability 14.43 mD) were compared, as shown in Fig. 12. In the rapid stage of imbibition, the macropores (1–8.617 μm) and transitional pores (0.01–0.1 μm) calculated by the two models have almost equal contributions to the imbibition recovery. But for transitional pores (0.01–0.1 μm), if the heterogeneity of pore seepage channels is not considered, the contribution to the recovery will be reduced by 2.91%.

In the transitional and slow stages of imbibition, if the heterogeneity of pore seepage channels is ignored, the calculated contributions of mesopores (0.1–1 μm) and transitional pores (0.01–0.1 μm) to imbibition recovery are reduced by 1.85% and 6.24%, respectively, as shown in Fig. 12(c) and (d).

If the heterogeneity of pore seepage channels is neglected, the calculation of oil recovery in pores 0.01–0.1 μm and 0.1–1 μm will deviate, resulting in the reduction of oil recovery in transitional pores and mesopores by 7.54% and 4.26%, respectively, as shown in

Fig. 13. The research results indicate that for low-permeability reservoirs, the production of oil in transitional pores and mesopores plays a crucial role in the late stage of imbibition, as shown in Fig. 12(c) and (d). Therefore, it is necessary to consider the heterogeneity of pore seepage channels in low-permeability reservoirs.

The research results show that for tight reservoirs (0–1 mD) the SI model constructed using single/average capillary tortuosity can characterize the imbibition process. This is why, the imbibition fractal models developed by Li et al. (2022), Wang and Zhao (2019), and Salam and Wang (2022) for tight or shale oil reservoirs, although they did not consider heterogeneity of pore seepage channels, still have a very high coefficient of determination.

The heterogeneity of the core is predominantly based on the range and concentration of pore radius sizes within the core. First, the standard deviation (s^2) of the pore radius is calculated, as shown in Eq. (28). According to the research, when $s^2 \ll 0.1$, the pore radius is concentrated; when $0.1 < s^2 < 5$, the pore radius is different; when $s^2 > 5$, the pore radius sizes exhibit significant heterogeneity. The discreteness of pore distribution was evaluated based on fractal dimension (D_f), as shown in Eq. (5). Research shows that when $D_f < 1.5$, the pore distribution is uniform, and when $D_f > 1.5$, the pore distribution is discrete.

$$s^2 = \frac{\sum_{i=1}^{m} (r_i - r_{av})^2}{m-1} \tag{28}$$

where s^2 is the standard deviation; m is the number of different pore radii; r_i is the pore radius, μm; r_{av} is the average pore radius, μm.

Therefore, when the $s^2 > 5$ and $D_f > 1.5$, the core is considered to exhibit heterogeneity. The heterogeneity of pore seepage channels must be considered in the process of calculating imbibition recovery. The new SI model considering the heterogeneity of pore seepage channels proposed in this paper improves the predictive accuracy of the imbibition process for low-permeability reservoirs by 2.58 times.

4.3. Influence of the threshold pressure on SI model

After considering the heterogeneity of pore seepage channels, although the determination coefficient of the core with permeability of 14.43 and 56.81 mD can be effectively increased by 1.18 and 2.58 times, respectively. The determination coefficients are 0.902 and 0.885, indicating that the characterization of the SI process is not accurate enough.

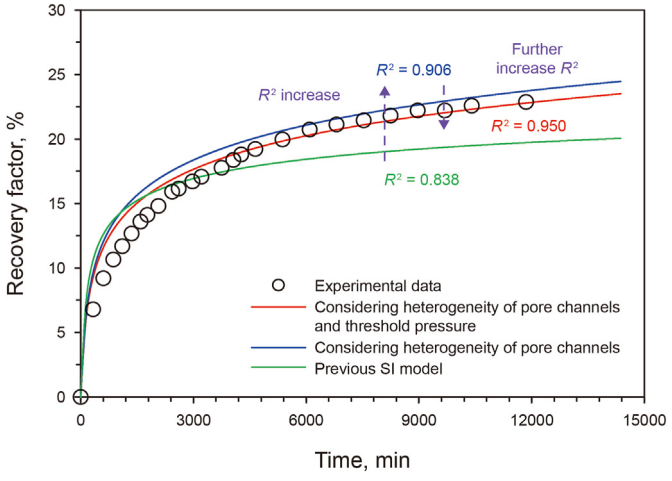

Fig. 14. Comparison of the imbibition profiles of SI recovery versus time with and without considering the threshold pressure, with core permeability of 10.12 mD.

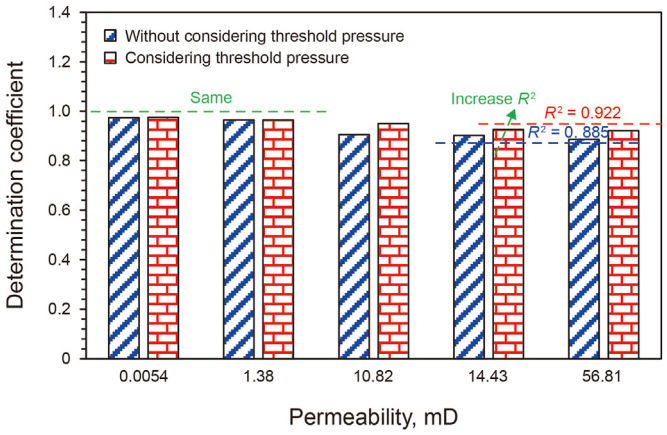

Fig. 15. Comparison of the determination coefficient of SI model with and without considering the threshold pressure for different permeability cores.

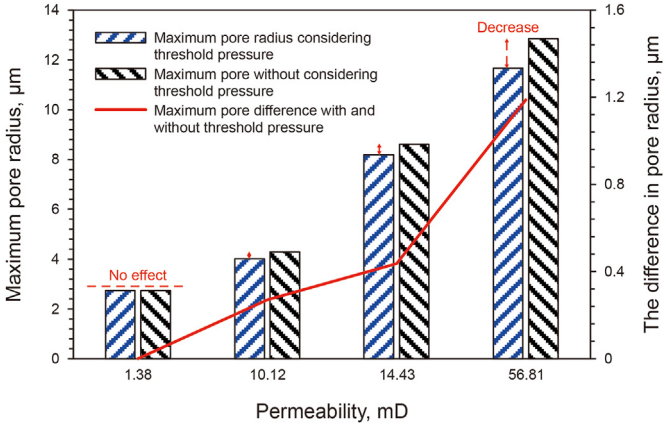

Fig. 16. Influence of threshold pressure on pore of oil production.

Only when the capillary force in the pores is higher than the threshold pressure the oil in the pores will be driven out. Therefore, in low-permeability reservoirs, the threshold pressure cannot be ignored. In this paper, on the basis of the SI model considering the heterogeneity of pore seepage channels, the influence of threshold pressure on SI model is added.

Based on the threshold pressure experiment, further imbibition experiment was conducted on core 4. The prediction accuracy of the SI model with and without considering the threshold pressure was compared, as shown in Fig. 14. The determination coefficient of the SI model considering heterogeneity of pore seepage channels is 0.906. On this basis, after considering the threshold pressure, the determination coefficient increases to 0.950, which is 1.05 times higher.

The viscosity of the oil used in cores L1, L4, L5 and L6 in the literature is 2.21, 2.90, 3.90 and 3.60 mPa s, respectively, which are similar to the viscosity of the experimental oil in the paper. Therefore, it is considered that the threshold pressure of these cores conforms to Eq. (1). The threshold pressure of these cores is calculated based on Eq. (1), and then apply to the new SI model, that considers threshold pressure and heterogeneity of pore seepage channels.

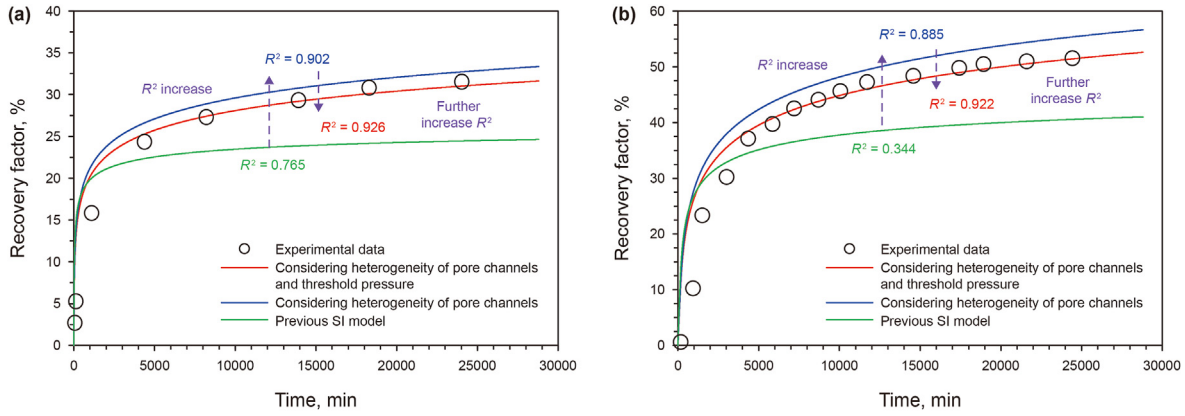

Fig. 17. Comparison of the SI model with and without considering the threshold pressure for cores L5 (**a**) and L6 (**b**).

Based on the SI model considering the heterogeneity of pore seepage channels, the influence of the threshold pressure on the determination coefficient of the SI model is further studied, as shown Fig. 15. When the permeability is less than 1.38 mD, the threshold pressure has no effect on the determination coefficient of the SI model. However, when the core permeability is higher than 10 mD, the determination coefficient of the SI model without considering the threshold pressure gradually decreases, and the minimum decreases to 0.885. For the new SI model considering the threshold pressure, the determination coefficient remains above 0.922.

As the pore radius increases, the capillary force and the pore number decrease, so that the imbibition force provided by the capillary bundle decreases. For these two reasons, in some large pores, the capillary force is smaller than the threshold pressure, causing the oil inside to be unrecoverable. Therefore, for low-permeability reservoirs, the effect of threshold pressure on imbibition recovery should be considered.

The effect of threshold pressure on oil recovery in pores of different scales was further studied, as shown in Fig. 16. For core L2, the threshold pressure has no effect on the production of oil in the pores. However, for core 4, the threshold pressure prevents the production of oil in pores of a diameter of 4.025–4.29 μm, and for core L5, oil in pores of a diameter of 8.183–8.617 μm cannot be produced. The effect of the threshold pressure on the mobilization of oil within the pores of core L6 is the most significant, and the oil in the pores of a diameter of 11.671–12.858 μm cannot be produced.

For core L5, after considering the threshold pressure, the determination coefficient is improved from 0.902 to 0.926, and its accuracy is increased by 1.03 times, as shown in Fig. 17(a). For core L6, after considering the threshold pressure, the determination coefficient is improved from 0.885 to 0.922, by 1.04 times, as shown in Fig. 17(b).

Taking core L6 as an example, after considering the heterogeneity of pore seepage channels, the determination coefficient increases from 0.344 to 0.885, increasing 2.58 times, and after considering the threshold pressure on the basis, the determination

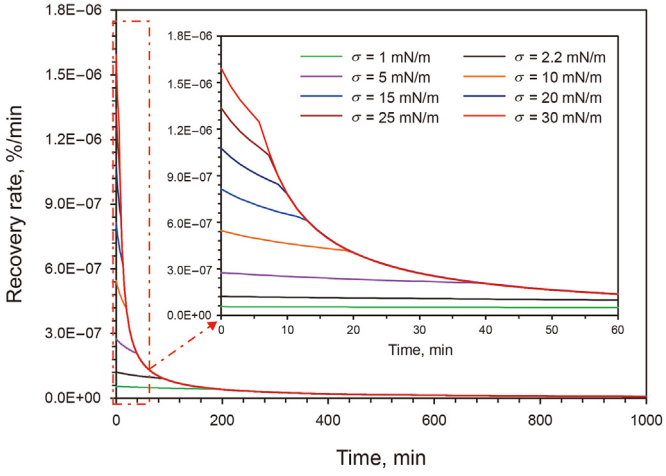

Fig. 19. Imbibition recovery rates for the cases with different IFT.

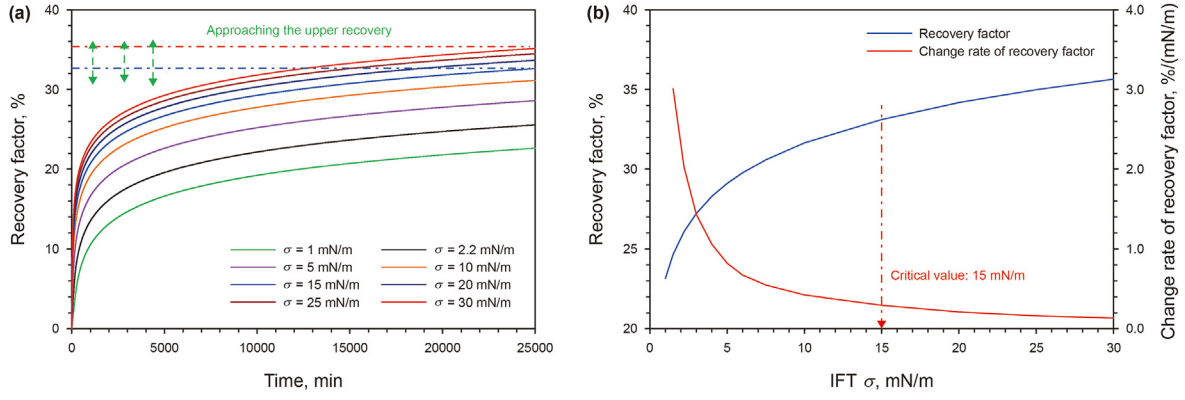

Fig. 18. Imbibition recovery factors for the cases with different IFT. (**a**) SI process of different IFT; (**b**) Effect of IFT on SI recovery.

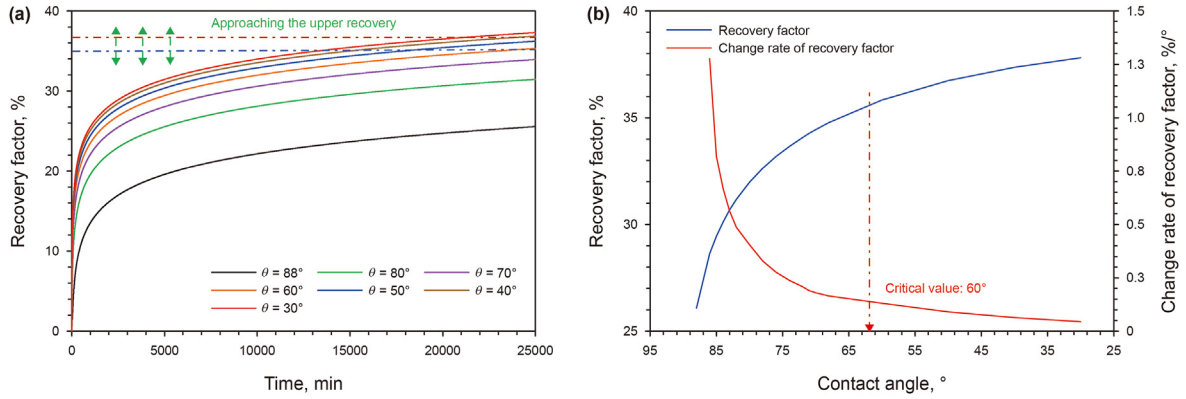

Fig. 20. Imbibition recovery factors for the cases with different wettability. (**a**) SI process of different contact angle values; (**b**) Effect of contact angle on SI recovery.

coefficient increases from 0.885 to 0.922, increasing 1.04 times, as shown in Fig. 17(b). For cores 4 and L5, there are similar results to core L6, as shown in Figs. 14 and 17(a).

The research shows that heterogeneity of pore seepage channels and threshold pressure affect the imbibition recovery of cores with permeability of 10–56.81 mD. Therefore, the new SI model considering heterogeneity of pore seepage channels and threshold pressure is more accurate in the characterization of imbibition in low-permeability reservoirs, increasing 5.68 times.

4.4. Sensitivity analysis

4.4.1. Effect of IFT on imbibition recovery

As shown in Fig. 18, as the IFT decreases from 1 to 30 mN/m, the imbibition recovery increases from 22.6% to 35.1%. This is because the capillary force is the driving force of imbibition, and as the IFT decreases, the driving force gradually decreases, making it difficult to produce oil in some pores.

As shown in Fig. 18(a), when the IFT increases from 15 to 30 mN/m, the imbibition recovery only increases by 2.51%, and taking IFT as the variable, the derivative of recovery factor change is 0.209. Therefore, 15 mN/m is referred to as the critical value of imbibition IFT.

When the IFT is higher than the critical value (15 mN/m), increasing the IFT has little effect on imbibition recovery. However, when the IFT is higher than the critical value, it can significantly increase the recovery rate in the early stage of imbibition, as shown in Fig. 19.

4.4.2. Effect of wettability on imbibition recovery

As shown in Fig. 20(a), as the contact angle decreases from 88° to 30°, the imbibition recovery increases from 25.5% to 37.3%. Changing the wettability of the reservoir can effectively improve the imbibition recovery, as demonstrated by the experimental results (Sun et al., 2021; Liu et al., 2019). When the contact angle decreases from 60° to 30°, the imbibition recovery increases only by 1.98%, and taking contact angle as the variable, the derivative of recovery factor change is 0.131. This indicates that when the contact angle is less than 60°, the effect of continuously reducing the contact angle on improving imbibition recovery is not obvious. Therefore, there is a critical value of 60° for contact angle to increase the imbibition recovery.

Most reservoirs are oil-wet or mixed-wet, so surfactants are added to the imbibition fluid to change reservoir wettability. While improving wettability, surfactants also reduce IFT between oil and water (Liu and Sheng, 2019). The results of this study indicate that the optimal surfactant for imbibition in low-permeability reservoirs can be selected by maintaining the IFT and contact angle above the critical value. The critical values of IFT and contact angle obtained from research effectively expand the range of surfactant selection for SI-EOR.

4.4.3. Effect of oil–water viscosity ratio on imbibition recovery

In the imbibition model, the viscosity of the water phase is kept constant (1 mPa s) and the viscosity of the oil was increased from 1.5 to 30 mPa s. Therefore, in the SI model, the oil–water viscosity ratio (μ_o/μ_w) can be adjusted from 1.5 to 30. The imbibition recovery under different oil–water ratios were calculated using the

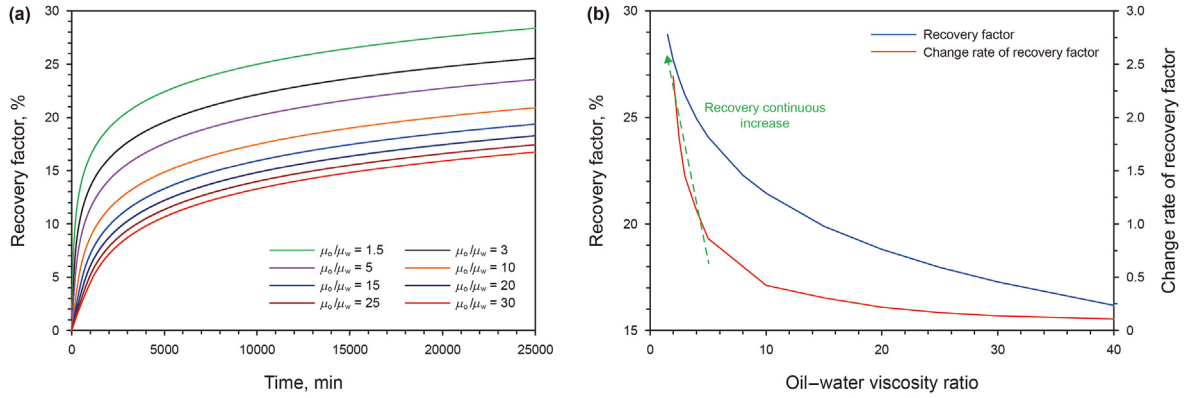

Fig. 21. Imbibition recovery factors for the cases with different oil–water viscosity ratios. (**a**) SI process of different viscosity; (**b**) Effect of viscosity on SI recovery.

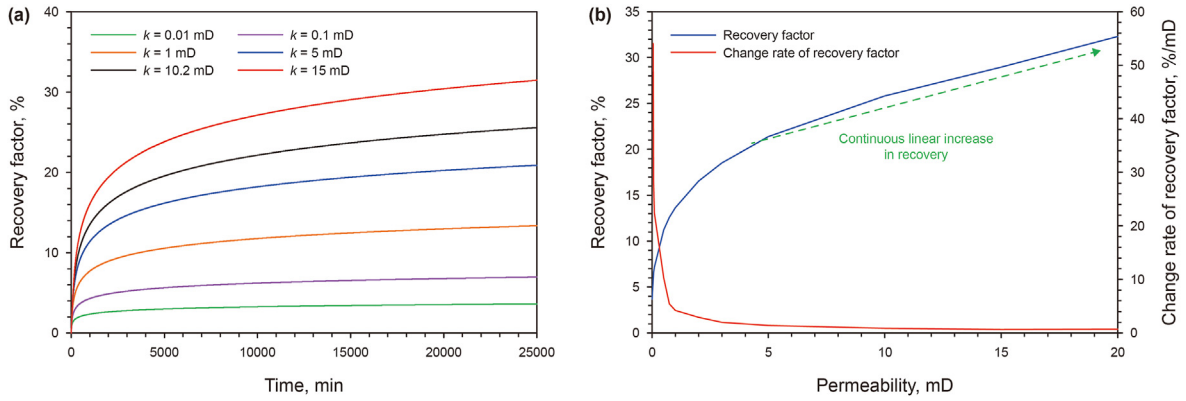

Fig. 22. Imbibition recovery factors for the cases with different permeability. (**a**) SI process of different permeability; (**b**) Effect of permeability on SI recovery.

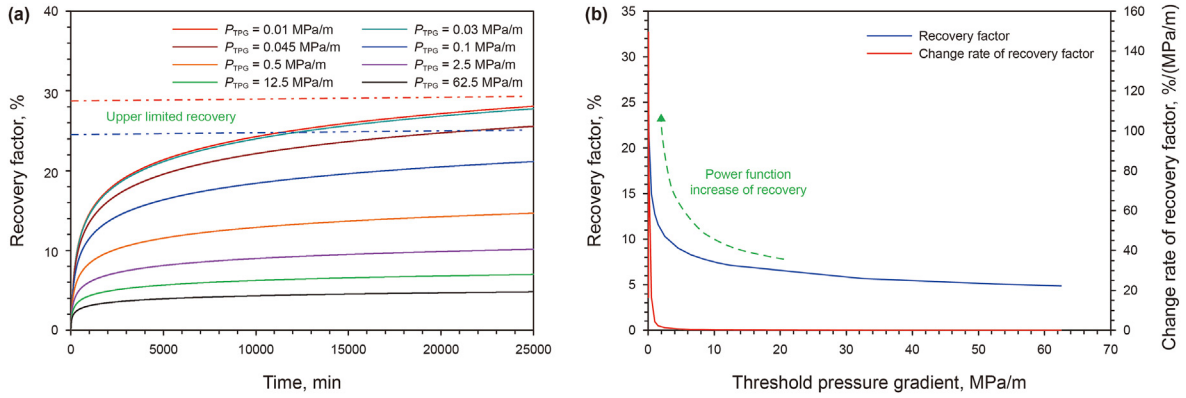

Fig. 23. Imbibition recovery factors for the cases with threshold pressure gradients. (**a**) SI process of different threshold pressure gradients; (**b**) Effect of threshold pressure gradient on SI recovery.

new SI model.

When the oil–water viscosity ratio decreases from 30 to 1.5, the imbibition recovery increases from 16.8% to 28.4%, as shown in Fig. 21(a). As the oil–water viscosity ratio decreases, the imbibition recovery will continue to increase, as shown in Fig. 21(b). Therefore, the optimal oil–water viscosity is 1.5. As the viscosity of the oil increases, the viscous force of the oil gradually increases, resulting in an increase in imbibition resistance, which causes a decrease in the imbibition recovery. Reducing oil viscosity by adding viscosity reducer can effectively improve imbibition recovery.

4.4.4. Effect of permeability on imbibition recovery

The imbibition recovery of cores with permeability ranging from 0.01 to 15 mD was calculated using the new SI model proposed in this paper. As the permeability increases from 0.01 to 15 mD, the imbibition recovery increases from 3.63% to 31.5%, as shown in Fig. 22.

With the increase in permeability, the pore connectivity increases and the seepage resistance inside the core decreases. So, the imbibition recovery gradually increases with the increase in core permeability (Yang et al., 2023). The recovery factor change rate is proportional to the core permeability. When the core permeability is higher than 10 mD, the recovery increases linearly with the increase in permeability.

4.4.5. Effect of the threshold pressure on imbibition recovery

According to the empirical formula obtained from the threshold pressure gradient experiment in this paper, the influence of threshold pressure on imbibition recovery was studied using the new SI model.

The imbibition recovery of cores with different threshold pressure gradients (0.01–62.5 MPa/m) was calculated, as shown in Fig. 23. When the threshold pressure gradient is 0.01 MPa/m, the imbibition recovery is 27.8%, and when the threshold pressure gradient is 62.5 MPa/m, imbibition recovery is 4.81%. This is because as the threshold pressure increases, some of the oil in the pores cannot be displaced under capillary forces.

The relationship between SI recovery and threshold pressure gradient is a power function, as shown in Fig. 23(b). When the threshold pressure gradient increases from 0.01 to 10 MPa/m, the imbibition recovery will decrease rapidly. When the threshold pressure gradient is higher than 10 MPa/m, the imbibition recovery decreases slowly. At the same time, due to the increase in seepage resistance, the recovery rate in the early stage of imbibition decreases. The research results further show that for low-permeability reservoirs, the effect of threshold pressure on imbibition recovery must be considered.

5. Conclusions

Based on the capillary model and fractal theory, this paper proposes a new SI mathematical model considering the heterogeneity of pore channels and the threshold pressure for low-permeability reservoirs. The new model was validated by imbibition experimental data. Comparing the new proposed model with the previous models, it is proved that the new model has higher

reliability in predicting the imbibition process of low-permeability reservoirs. The sensitivity analysis evaluated the impact of IFT, contact angle, and oil–water viscosity ratio on SI recovery. The following conclusions can be drawn from this study:

(1) The previous SI model based on the single/average capillary tortuosity can accurately predict the imbibition recovery of cores with permeability from 0.0054 to 1.38 mD, and its determination coefficient is 0.967–0.903. However, the imbibition simulation of cores with permeability from 10.12 to 56.8 mD is only 0.765–0.344. Ignoring the heterogeneity of pore seepage channels, the previous SI model underestimates the contribution of transitional pores and mesopores to SI recovery, reducing 7.54% and 4.26%, respectively.
(2) For cores with permeability from 0.0054 to 1.38 mD, the new SI model considering heterogeneity of pore seepage channels can effectively increase the determination coefficient by 1.07 times. For cores with permeability from 10.12 to 56.82 mD, the new model can greatly increase the coefficient of determination by 1.05–2.58 times. And on this basis, considering the threshold pressure, the coefficient of determination can be further increased by 1.05 times. Heterogeneity of pore seepage channels and threshold pressure affect imbibition recovery in low-permeability reservoirs.
(3) Increasing IFT, decreasing contact angle and viscosity ratio can effectively improve the recovery of imbibition in low-permeability reservoirs. There are critical values for the three influencing factors: IFT is 15 mN/m, contact angle is 60°, and oil–water viscosity ratio is 1.5. The existence of critical points provides new theoretical support for the optimal selection of surfactants.

CRediT authorship contribution statement

Ming-Sheng Zuo: Methodology, Validation, Writing – original draft, Writing – review & editing. **Hao Chen:** Supervision, Writing – review & editing. **Xi-Liang Liu:** Supervision, Validation. **Hai-Peng Liu:** Investigation, Validation. **Yi Wu:** Investigation, Validation. **Xin-Yu Qi:** Investigation.

Declaration of competing interest

The authors declare that they have no known competing financial interests or personal relationships that could have appeared to influence the work reported in this paper.

Acknowledgments

This work is supported by China Natural Science Foundation (Grant No. 52274053), Beijing Natural Science Foundation (Grant No. 3232028), and Open Fund of State Key Laboratory of Offshore Oil Exploitation (Grant No. CCL2021RCPS0515KQN).

References

Adibhatla, B., Mohanty, K.K., 2008. Oil recovery from fractured carbonates by surfactant-aided gravity drainage: laboratory experiments and mechanistic simulations. SPE Reservoir Eval. Eng. 11 (1), 119–130. https://doi.org/10.2118/99773-PA.

Adibhatla, B., Sun, X., Mohanty, K.K., 2005. Numerical studies of oil production from initially oil-wet fracture blocks by surfactant brine imbibition. In: SPE International Improved Oil Recovery Conference in Asia Pacific. https://doi.org/10.2118/97687-MS.

Al-Gharbi, M.S., Blunt, M.J., 2005. Dynamic network modeling of two-phase drainage in porous media. Phys. Rev. 71 (1), 016308. https://doi.org/10.1103/PhysRevE.71.016308.

Allan, J., Sun, S.Q., 2003. Controls on recovery factor in fractured reservoirs: lessons learned from 100 fractured fields. In: SPE Annual Technical Conference and Exhibition. https://doi.org/10.2118/84590-MS.

Bauer, D., Talon, L., Peysson, Y., et al., 2019. Experimental and numerical determination of Darcy's law for yield stress fluids in porous media. Phys. Rev. Fluids 4 (6), 063301. https://doi.org/10.1103/PhysRevFluids.4.063301.

Buiting, J.J.M., Clerke, E.A., 2013. Permeability from porosimetry measurements: derivation for a tortuous and fractal tubular bundle. J. Petrol. Sci. Eng. 108, 267–278. https://doi.org/10.1016/j.petrol.2013.04.016.

Cai, J., Yu, B., 2010. Prediction of maximum pore size of porous media based on fractal geometry. Fractals 18 (4), 417–423. https://doi.org/10.1142/S0218348X10005123.

Cai, J., Yu, B., 2011. A discussion of the effect of tortuosity on the capillary imbibition in porous media. Transport Porous Media 89 (2), 251–263. https://doi.org/10.1007/s11242-011-9767-0.

Cai, J., Hu, X., Standnes, D.C., et al., 2012. An analytical model for spontaneous imbibition in fractal porous media including gravity. Colloids Surf. A Physicochem. Eng. Asp. 414, 228–233. https://doi.org/10.1016/j.colsurfa.2012.08.047.

Cao, G., Cheng, Q., Liu, Y., et al., 2022. Influencing factors of surfactant stripping crude oil and spontaneous imbibition mechanism of surfactants in a tight reservoir. ACS Omega 7 (22), 19010–19020. https://doi.org/10.1021/acsomega.2c02190.

Chen, H., Xing, J., Jiang, D., et al., 2022. A fractal model of low-velocity non-Darcy flow considering viscosity distribution and boundary layer effect. Fractals 30 (1), 2250006. https://doi.org/10.1142/S0218348X22500062.

Cheng, Z., Wang, Q., Ning, Z., et al., 2018. Experimental investigation of countercurrent spontaneous imbibition in tight sandstone using nuclear magnetic resonance. Energy Fuels 32 (6), 6507–6517. https://doi.org/10.1021/acs.energyfuels.8b00394.

Dai, C., Cheng, R., Sun, X., et al., 2019. Oil migration in nanometer to micrometer sized pores of tight oil sandstone during dynamic surfactant imbibition with online NMR. Fuel 245, 544–553. https://doi.org/10.1016/j.fuel.2019.01.021.

Das, S., Adeoye, J., Dhiman, I., et al., 2019. Imbibition of mixed-charge surfactant fluids in shale fractures. Energy Fuels 33 (4), 2839–2847. https://doi.org/10.1021/acs.energyfuels.8b03447.

Dong, M., Dullien, F.L., Zhou, J., 1998. Characterization of waterflood saturation profile histories by the 'complete' capillary number. Transport Porous Media 31, 213–237.

El-Amin, M.F., Salama, A., Sun, S., 2013. Numerical and dimensional investigation of two-phase countercurrent imbibition in porous media. J. Comput. Appl. Math. 242, 285–296. https://doi.org/10.1016/j.cam.2012.09.035.

Gao, Y., Wu, K., Chen, Z., et al., 2021. Effect of wetting hysteresis on fluid flow in shale oil reservoirs. Energy Fuels 35 (15), 12075–12082. https://doi.org/10.1021/acs.energyfuels.1c01697.

Gupta, R., Mohanty, K.K., 2010. Temperature effects on surfactant-aided imbibition into fractured carbonates. SPE J. 15 (3), 588–597. https://doi.org/10.2118/110204-PA.

Higgs, K.E., Zwingmann, H., Reyes, A.G., et al., 2007. Diagenesis, porosity evolution, and petroleum emplacement in tight gas reservoirs, Taranaki Basin, New Zealand. J. Sediment. Res. 77 (12), 1003–1025. https://doi.org/10.2110/jsr.2007.095.

Javaheri, A., Habibi, A., Dehghanpour, H., et al., 2018. Imbibition oil recovery from tight rocks with dual-wettability behavior. J. Petrol. Sci. Eng. 167, 180–191. https://doi.org/10.1016/j.petrol.2018.01.046.

Kalaei, M.H., Green, D.W., Willhite, G.P., 2013. A new dynamic wettability-alteration model for oil-wet cores during surfactant-solution imbibition. SPE J. 18 (5), 818–828. https://doi.org/10.2118/153329-PA.

Katz, A.J., Thompson, A.H., 1985. Fractal sandstone pores: implications for conductivity and pore formation. Phys. Rev. Lett. 54 (12), 1325. https://doi.org/10.1103/PhysRevLett.54.1325.

Leclaire, S., Parmigiani, A., Malaspinas, O., et al., 2017. Generalized three-dimensional lattice Boltzmann color-gradient method for immiscible two-phase pore-scale imbibition and drainage in porous media. Phys. Rev. 95 (3), 033306. https://doi.org/10.1103/PhysRevE.95.033306.

Li, C., Xian, C., Ge, H., et al., 2022. The mechanism analysis for hemiwicking on spontaneous imbibition in tight sandstone based on intermingled fractal model. J. Petrol. Sci. Eng. 213, 110437. https://doi.org/10.1016/j.petrol.2022.110437.

Li, D., Zha, W., Liu, S., et al., 2016. Pressure transient analysis of low permeability reservoir with pseudo threshold pressure gradient. J. Petrol. Sci. Eng. 147, 308–316. https://doi.org/10.1016/j.petrol.2016.05.036.

Li, K., 2010. Analytical derivation of Brooks–Corey type capillary pressure models using fractal geometry and evaluation of rock heterogeneity. J. Petrol. Sci. Eng. 73 (1–2), 20–26. https://doi.org/10.1016/j.petrol.2010.05.002.

Liu, J., Sheng, J.J., 2019. Experimental investigation of surfactant enhanced spontaneous imbibition in Chinese shale oil reservoirs using NMR tests. J. Ind. Eng. Chem. 72, 414–422. https://doi.org/10.1016/j.jiec.2018.12.044.

Liu, J., Sheng, J.J., Tu, J., 2020. Effect of spontaneous emulsification on oil recovery in tight oil-wet reservoirs. Fuel 279, 118456. https://doi.org/10.1016/j.fuel.2020.118456.

Liu, J., Sheng, J.J., Wang, X., et al., 2019. Experimental study of wettability alteration and spontaneous imbibition in Chinese shale oil reservoirs using anionic and nonionic surfactants. J. Petrol. Sci. Eng. 175, 624–633. https://doi.org/10.1016/j.petrol.2019.01.003.

Lu, S., Li, J., Zhang, P., et al., 2018. Classification of microscopic pore-throats and the grading evaluation on shale oil reservoirs. Petrol. Explor. Dev. 45 (3), 452–460.

https://doi.org/10.1016/S1876-3804(18)30050-8.
Lucas, R., 1918. Rate of capillary ascension of liquids. Kolloid Z. 23 (15), 15–22.
Lux, J., Anguy, Y., 2012. A study of the behavior of implicit pressure explicit saturation (IMPES) schedules for two-phase flow in dynamic pore network models. Transport Porous Media 93 (1), 203–221. https://doi.org/10.1007/s11242-012-9952-9.
Mason, G., Morrow, N.R., 2013. Developments in spontaneous imbibition and possibilities for future work. J. Petrol. Sci. Eng. 110, 268–293. https://doi.org/10.1016/j.petrol.2013.08.018.
Meng, Q., Liu, H., Wang, J., 2017. A critical review on fundamental mechanisms of spontaneous imbibition and the impact of boundary condition, fluid viscosity and wettability. Adv. Geo-Energy Res. 1 (1), 1–17. https://doi.org/10.26804/ager.2017.01.01.
Meng, Q., Cai, Z., Cai, J., et al., 2019. Oil recovery by spontaneous imbibition from partially water-covered matrix blocks with different boundary conditions. J. Petrol. Sci. Eng. 172, 454–464. https://doi.org/10.1016/j.petrol.2018.09.075.
Miller, R.J., Low, P.F., 1963. Threshold gradient for water flow in clay systems. Soil Sci. Soc. Am. J. 27 (6), 605–609. https://doi.org/10.2136/sssaj1963.03615995002700060013x.
Mirzaei-Paiaman, A., Masihi, M., Standnes, D.C., 2013. Index for characterizing wettability of reservoir rocks based on spontaneous imbibition recovery data. Energy Fuels 27 (12), 7360–7368. https://doi.org/10.1021/ef401953b.
Morrow, N.R., Mason, G., 2001. Recovery of oil by spontaneous imbibition. Curr. Opin. Colloid Interface Sci. 6 (4), 321–337. https://doi.org/10.1016/S1359-0294(01)00100-5.
Øren, P.E., Bakke, S., Arntzen, O.J., 1998. Extending predictive capabilities to network models. SPE J. 3 (4), 324–336. https://doi.org/10.2118/52052-PA.
Porter, M.L., Schaap, M.G., Wildenschild, D., 2009. Lattice-Boltzmann simulations of the capillary pressure–saturation–interfacial area relationship for porous media. Adv. Water Resour. 32 (11), 1632–1640. https://doi.org/10.1016/j.advwatres.2009.08.009.
Prada, A., Civan, F., 1999. Modification of Darcy's law for the threshold pressure gradient. J. Petrol. Sci. Eng. 22 (4), 237–240. https://doi.org/10.1016/S0920-4105(98)00083-7.
Ruth, D., Bartley, J., 2011. Capillary tube models with interaction between the tubes [a note on "immiscible displacement in the interacting capillary bundle model part I. development of interacting capillary bundle model", by Dong, M., Dullien, F.A.L., Dai, L. and Li, D., 2005, Transport Porous Media]. Transport Porous Media 86 (2), 479–482. https://doi.org/10.1007/s11242-010-9633-5.
Salam, A., Wang, X., 2022. An analytical solution on spontaneous imbibition coupled with fractal roughness, slippage and gravity effects in low permeability reservoir. J. Petrol. Sci. Eng. 208, 109501. https://doi.org/10.1016/j.petrol.2021.109501.
Sang, Q., Zhao, X.Y., Liu, H.M., et al., 2022. Analysis of imbibition of n-alkanes in kerogen slits by molecular dynamics simulation for characterization of shale oil rocks. Petrol. Sci. 19 (3), 1236–1249. https://doi.org/10.1016/j.petsci.2022.01.005.
Seethepalli, A., Adibhatla, B., Mohanty, K.K., 2004. Physicochemical interactions during surfactant flooding of fractured carbonate reservoirs. SPE J. 9 (4), 411–418. https://doi.org/10.2118/89423-PA.
Souayeh, M., Al-Maamari, R.S., Karimi, M., et al., 2021. Wettability alteration and oil recovery by surfactant assisted low salinity water in carbonate rock: the impact of nonionic/anionic surfactants. J. Petrol. Sci. Eng. 197, 108108. https://doi.org/10.1016/j.petrol.2020.108108.
Sun, D., Zou, C., Jia, A., et al., 2019. Development characteristics and orientation of tight oil and gas in China. Petrol. Explor. Dev. 46 (6), 1015–1026. https://doi.org/10.1016/S1876-3804(19)60264-8.
Sun, Y.P., Xin, Y., Lyu, F.T., et al., 2021. Experimental study on the mechanism of adsorption-improved imbibition in oil-wet tight sandstone by a nonionic surfactant for enhanced oil recovery. Petrol. Sci. 18 (4), 1115–1126. https://doi.org/10.1016/j.petsci.2021.07.005.
Tian, W., Li, A., Ren, X., et al., 2018. The threshold pressure gradient effect in the tight sandstone gas reservoirs with high water saturation. Fuel 226, 221–229. https://doi.org/10.1016/j.fuel.2018.03.192.
Tian, W., Wu, K., Chen, Z., et al., 2021. Effect of dynamic contact angle on spontaneous capillary-liquid-liquid imbibition by molecular kinetic theory. SPE J. 26 (4), 2324–2339. https://doi.org/10.2118/205490-PA.
Tørå, G., Øren, P.E., Hansen, A., 2012. A dynamic network model for two-phase flow in porous media. Transport Porous Media 92, 145–164. https://doi.org/10.1007/s11242-011-9895-6.
Wang, F., Liu, Z., Jiao, L., et al., 2017. A fractal permeability model coupling boundary-layer effect for tight oil reservoirs. Fractals 25 (5), 1750042. https://doi.org/10.1142/S0218348X17500426.
Wang, F., Zhao, J., 2019. A mathematical model for co-current spontaneous water imbibition into oil-saturated tight sandstone: upscaling from pore-scale to core-scale with fractal approach. J. Petrol. Sci. Eng. 178, 376–388. https://doi.org/10.1016/j.petrol.2019.03.055.
Wang, Z., Guo, H., You, J., et al., 2022. Effect of surfactant on imbibition and displacement in ultra-low permeability reservoir. Unconventional Oil Gas 9 (1), 77–83. https://doi.org/10.19901/j.fcgyq.2022.01.10 (in Chinese).
Washburn, E.W., 1921. The dynamics of capillary flow. Phys. Rev. 17 (3), 273. https://doi.org/10.1103/PhysRev.17.273.
Wu, R., Yang, S., Xie, J., et al., 2017. Experiment and mechanism of spontaneous imbibition of matrix core in tight oil-gas reservoirs. Editorial Depart. Petrol. Geol. Recovery Efficiency 24 (3), 98–104. https://doi.org/10.13673/j.cnki.cn37-1359/te.2017.03.015 (in Chinese).
Wu, Z., Cui, C., Ye, Y., et al., 2021. A fractal model for quantitative evaluating the effects of spontaneous imbibition and displacement on the recovery of tight reservoirs. J. Petrol. Sci. Eng. 198, 108120. https://doi.org/10.1016/j.petrol.2020.108120.
Xu, D., Bai, B., Wu, H., et al., 2019. Mechanisms of imbibition enhanced oil recovery in low permeability reservoirs: effect of IFT reduction and wettability alteration. Fuel 244, 110–119. https://doi.org/10.1016/j.fuel.2019.01.118.
Xu, P., Yu, B., 2008. Developing a new form of permeability and Kozeny–Carman constant for homogeneous porous media by means of fractal geometry. Adv. Water Resour. 31 (1), 74–81. https://doi.org/10.1016/j.advwatres.2007.06.003.
Yang, K., Wang, F.Y., Zhao, J.Y., 2023. Experimental study of surfactant-enhanced spontaneous imbibition in fractured tight sandstone reservoirs: the effect of fracture distribution. Petrol. Sci. 20 (1), 370–381. https://doi.org/10.1016/j.petsci.2022.09.033.
Yang, L., Wang, H., Zou, Z., et al., 2021. Effects of fracture characteristics on spontaneous imbibition in a tight reservoir. Energy Fuels 35 (19), 15995–16006. https://doi.org/10.1021/acs.energyfuels.1c01831.
Yassin, M.R., Dehghanpour, H., Begum, M., et al., 2018. Evaluation of imbibition oil recovery in the Duvernay formation. SPE Reservoir Eval. Eng. 21 (2), 257–272. https://doi.org/10.2118/185065-PA.
Yu, B., 2008. Analysis of flow in fractal porous media. Appl. Mech. Rev. 61 (5), 050801. https://doi.org/10.1115/1.2955849.
Yu, B., Cheng, P., 2002. A fractal permeability model for bi-dispersed porous media. Int. J. Heat Mass Tran. 45 (14), 2983–2993. https://doi.org/10.1016/S0017-9310(02)00014-5.
Yu, B., Lee, L.J., Cao, H., 2002. A fractal in-plane permeability model for fabrics. Polym. Compos. 23 (2), 201–221. https://doi.org/10.1002/pc.10426.
Yu, B., Li, J., 2004. A geometry model for tortuosity of flow path in porous media. Chin. Phys. Lett. 21 (8), 1569. https://doi.org/10.1088/0256-307X/21/8/044.
You, Q., Wang, H., Zhang, Y., et al., 2018. Experimental study on spontaneous imbibition of recycled fracturing flow-back fluid to enhance oil recovery in low permeability sandstone reservoirs. J. Petrol. Sci. Eng. 166, 375–380. https://doi.org/10.1016/j.petrol.2018.03.058.
Zhou, Y., Helland, J.O., Hatzignatiou, D.G., 2014. Pore-scale modeling of waterflooding in mixed-wet-rock images: effects of initial saturation and wettability. SPE J. 19 (1), 88–100. https://doi.org/10.2118/154284-PA.
Zhu, Y., Li, Z., Ni, J., et al., 2022. Modeling the spontaneous imbibition of non-Newtonian fluids into the fractal porous media of tight reservoirs. J. Petrol. Sci. Eng. 209, 109892. https://doi.org/10.1016/j.petrol.2021.109892.
Zou, C., Zhu, R., Liu, K., et al., 2012. Tight gas sandstone reservoirs in China: characteristics and recognition criteria. J. Petrol. Sci. Eng. 88, 82–91. https://doi.org/10.1016/j.petrol.2012.02.001.